GEOPHYSICS, VOL. 75, NO. 4 (JULY-AUGUST 2010); P. WA17–WA25, 9 FIGS.
10.1190/1.3475533

Self-potential monitoring of a salt plume

P. Martínez-Pagán[1,2], A. Jardani[3], A. Revil[2,4], and A. Haas[2]

ABSTRACT

Nonintrusively monitoring the spread of contaminants in real time with a geophysical method is an important task in hydrogeophysics. We have developed a sandbox experiment showing that the self-potential method can locate both the source of leakage and the front of a contaminant plume. We monitored the leakage of a plume of salty water from a hole at the bottom of a small tank located at the top of a main sandbox. Initially, the sand was saturated by tap water. At a given time, a hole was opened at the bottom of the tank, allowing the salty water to migrate by diffusion and buoyancy-driven flow in the main sandbox. The bottom of the sandbox contained a network of 32 nonpolarizing silver-silver chloride electrodes with amplifiers, connected to a multichannel voltmeter. The self-potential response associated with the migration of the salt plume in the sandbox was recorded over time. A self-potential anomaly was observed with amplitude varying from a few millivolts at the start of the leak to a few tens of millivolts after a few minutes. The self-potential data were inverted using a time-lapse tomographic algorithm to reconstruct the position of the volumetric source current density over time. A positive volumetric source current density was associated with the position of the leak at the bottom of the leaking tank, whereas a negative volumetric source current density was associated with the salinity front moving down inside the sandbox. These poles were well reproduced by performing a finite-element simulation of the problem. Using this information, we estimated the speed of the salt plume sinking inside the sandbox. Therefore, the self-potential method can be used to track, in real time, the position of the front of a contaminant plume in a porous material.

INTRODUCTION

Ponds and lagoons lined with electrically resistive plastic liners often are used worldwide to store toxic and hazardous wastes or large quantities of solid and liquid wastes (Frangos, 1997; Darilek and Laine, 2007). In recent years, an increasing amount of work has shown the usefulness of electrical resistivity as a method to locate leakages from plastic liners. Because many stored wastes have a high electrical conductivity contrast with soil water, resistivity methods have been used in many studies. Parra (1988) and Parra and Owen (1988) describe, for instance, the use of a pole-dipole array making voltage measurements inside the pond to detect a current being driven through the leak (mise-à-la masse method) (see also Frangos, 1997, and Darilek and Laine, 2007). Binley et al. (1997) propose a tomographic electrical leak imaging system as a tomographic variant of traditional, permanently installed, electrical leak-location methods. Binley and Daily (2003) evaluate a model with 48 stainless steel electrodes for electrical imaging of a leaking landfill liner and a leaking landfill cap. Daily et al. (2004) use electrical resistance tomography (ERT) to map the spatial variations of electrical resistivity owing to any plume existing in the soil by using an array of electrodes in boreholes around a storage tank.

In the present work, we investigate the usefulness of the self-potential method to locate a leakage of highly conductive saline water from a tank. The self-potential method is a passive geophysical method evidencing the existence of electrical currents in the ground. The distribution of the electrical potential is passively recorded using a network of nonpolarizing electrodes. The in situ source of current responsible for the self-potential anomalies can be due to redox processes (Fox, 1830; Castermant et al., 2008; Revil et al., 2009), groundwater flow through an electrokinetic process (Fournier, 1989; Birch, 1993; Aubert and Atangana, 1996; Suski et al., 2004; Crespy et al., 2007; Malama et al., 2009a, 2009b), or the gradient in the chemical potential of the ions in the salty water (Maineult et al.,

Manuscript received by the Editor 1 July 2009; revised manuscript received 17 October 2009; published online 30 September 2010.
[1]Technical University of Cartagena, Department of Mining, Geology and Surveying, Cartagena, Murcia, Spain. E-mail: p.martinez@upct.es.
[2]Colorado School of Mines, Department of Geophysics, Golden, Colorado, U.S.A. E-mail: arevil@mines.edu; ahaas@mines.edu.
[3]Formerly Colorado School of Mines, Department of Geophysics, Golden, Colorado, U.S.A; presently Université de Rouen, Mont Saint Aignan, France. E-mail: ajardani@mines.edu.
[4]CNRS-UMR 5559-LGIT, Université de Savoie, Equipe Volcan, Le Bourget-du-lac, France.

2004, 2005, 2006; Revil and Linde, 2006; Revil et al., 2009). The self-potential has barely been used for monitoring the leakage from waste lined ponds. Nevertheless, some works have successfully delineated contaminant plumes from landfills (Weigel, 1989; Hämmann et al., 1997; Naudet et al., 2003; Naudet et al., 2004; Arora et al., 2007) and hydrocarbon-contaminated areas (Perry et al., 1996; Buselli and Lu, 2001).

We present a diffusion/infiltration (buoyancy-driven) experiment whereby we evaluate the capabilities of the self-potential method to locate the front of a salt plume leaking from a small container in a sandbox experiment. We develop the fundamental equations to simulate the self-potential signals associated with the transport of a plume of salty water. The resulting partial differential equations are solved with the finite-element code COMSOL Multiphysics 3.5 to perform a forward simulation of the problem that agrees with the observations. In addition, we propose a time-lapse tomographic algorithm to locate the front of the salt plume.

SELF-POTENTIAL MONITORING OF A SALT PLUME

We first recall the transport equations for the migration of a salt plume in a porous material. This problem requires the solution of the following set of equations (e.g., Oltean and Buès, 2002):

$$\mathbf{u} = \phi\mathbf{v} = -\frac{\mathbf{k}}{\eta_f}(\nabla p + \rho_f g \nabla z), \tag{1}$$

$$\frac{\partial(\rho_f\phi)}{\partial t} + \nabla\cdot(\rho_f\phi\mathbf{v}) = \rho_f Q_s, \tag{2}$$

$$\frac{\partial(\rho_f\phi C_m)}{\partial t} + \nabla\cdot(\rho_f\phi\mathbf{v}C_m) - \nabla\cdot[\rho_f\phi\mathbf{D}\nabla C_m] = \rho Q_s C_m^0 \tag{3}$$

$$\rho_f = \rho_f^0 + \gamma C_m, \tag{4}$$

$$\eta_f = \eta_f^0(1 + \tau_1 C_m + \tau_2 C_m{}^2 + \tau_3 C_m{}^3), \tag{5}$$

where $\mathbf{v}$ is the mean velocity of the pore water in the pore space (m s^{-1}); $\mathbf{k}$ is the permeability tensor (in m^2); ϕ is porosity; p is the pore fluid pressure (pascal); η_f is the dynamic viscosity of the pore fluid (in pascal s); ρ_f is the solute bulk density; ρ_f^0 is the bulk density of water (in kg m^{-3}); g is the acceleration of the gravity (in m s^{-2}); Q_S is a source term (in s^{-1}); C_m is the solute mass fraction (dimensionless); C_m^0 is the solute mass fraction in the source term; γ is a constant coefficient for the density law; and τ_1, τ_2, and τ_3 are the empirical constants for the viscosity law. Equation 1 represents the constitutive equation for the flow of the pore water (Darcy's law). Equation 2 is a continuity equation for the mass of the pore water. Equation 3 is the field equation for the salt concentration. Equations 4 and 5 are empirical equations connecting the mass density and the dynamic viscosity of the pore water to the salinity.

In the widely used Fickian model, the effective hydrodynamic dispersion tensor $\mathbf{D}$ (m^2 s^{-1}) entering equation 4 is given by

$$\mathbf{D} = [D_m + \alpha_T v]\mathbf{I} + \frac{\alpha_L - \alpha_T}{v}\mathbf{v}\mathbf{v}, \tag{6}$$

where D_m is the molecular diffusion coefficient of the salt and corrected for the effect of tortuosity (in m^2 s^{-1}) (see Revil et al., 2005); $\mathbf{I}$ is the unit tensor; and α_L and α_T are the longitudinal and transverse dispersivity (in m), respectively. Revil et al. (1996) and Revil (1999) developed a rigorous analysis of this coefficient generalizing the Nernst-Hartley equation for the diffusion of a binary salt in water to brine-saturated porous media. For a sodium chloride solution, the molecular diffusion coefficient of the salt is typically comprised between 1.60×10^{-9} m^2 s^{-1} at infinite dilution to 1.44×10^{-9} m^2 s^{-1} at high salinities. The tortuosity of the pore space is given by the product of the formation factor with the porosity and is equal to 1.6.

In the case of a salt plume moving in a porous material, there are two contributions of the source current density generating self-potential signals. The first contribution is associated with the flow of the pore water due to the gravity force and driven below by the difference of density between the salt plume and the surrounding freshwater. This contribution corresponds to the so-called streaming current density (e.g., Fournier, 1989; Birch, 1993; Aubert and Atangana, 1996; Revil and Leroy, 2001). The second contribution is related to the gradient of the salinity. It depends on the gradients of the activity of the charge carriers (ions) that are present in the pore water (e.g., Maineult et al., 2004, 2005, 2006; Revil and Leroy, 2004; Revil and Linde, 2006).

The total electrical current density $\mathbf{j}$ is given by (Sill, 1983)

$$\mathbf{j} = \sigma\mathbf{E} + \mathbf{j}_S, \tag{7}$$

$$\nabla\cdot\mathbf{j} = 0, \tag{8}$$

where $\mathbf{E}$ is the electrical field $\mathbf{E} = -\nabla\psi$, ψ is the electrical potential (in V), σ is the electrical conductivity of the porous material (in S m^{-1}), and $\mathbf{j}_s$ is the source current density (in A m^{-2}). Equation 7 is a generalized Ohm's law, and equation 8 is the continuity equation for the charge in the low-frequency limit of the Maxwell equations. The total source current density is given by (Revil and Linde, 2006)

$$\mathbf{j}_S = \bar{Q}_V\mathbf{u} - k_b T\sum_{i=1}^{N}\frac{t_i\sigma}{q_i}\nabla\ln\{i\}, \tag{9}$$

where T is the absolute temperature; k_b is the Boltzmann constant; $\bar{Q}_V$ is the effective charge per unit volume that can be dragged by the flow of the pore water; $\mathbf{u}$ represents the Darcy velocity; q_i is the charge of species i dissolved in water; t_i is the microscopic Hittorf number of the ionic species i in the pore water (that is, the fraction of electrical current carried by this species in the water phase); and $\{i\}$ represents the activity of the ionic species i (concentration times the activity coefficient). In the case reported below, the salt plume is characterized by two ionic species Na^+ and Cl^-, resulting from the total dissociation of NaCl. The first term of the right-hand side of equation 9 corresponds to the streaming current density, whereas the second term corresponds to the diffusion current density.

Revil (1999) showed that in a diffusion problem, one could replace the gradient of the logarithm of the activity of the salt by the gradient of the logarithm of the activity of the conductivity of the salt. Using this approach, we can rewrite the total source current as

$$\mathbf{j}_S = \bar{Q}_V \mathbf{u} - \frac{k_b T}{e} \sigma (2t_{(+)} - 1) \nabla \ln \sigma_f, \tag{10}$$

where e is the elementary charge of the electron; $t_{(+)}$ is the microscopic Hittorf number of the cation (see values in Revil, 1999, $t_{(+)} = 0.38$ for a sodium chloride solution); and σ_f is the conductivity of the pore water, which is proportional to the salinity at a given temperature. In clean sand at low Dukhin numbers (e.g., Bolève et al., 2007; Crespy et al., 2008), the conductivity of the sand is given by the following well-known relationship

$$\sigma = \frac{\sigma_f}{F}, \tag{11}$$

where F is the electrical formation factor (dimensionless). The formation factor usually is related to porosity ϕ by Archie's law $F = \phi^{-m}$, where m is the cementation exponent (typically 1.3 for a well-sorted clean sand). From equations 10 and 11, the total source current density can be rewritten as

$$\mathbf{j}_S = \bar{Q}_V \mathbf{u} - \frac{k_b T}{Fe} (2t_{(+)} - 1) \nabla \sigma_f, \tag{12}$$

$$\mathbf{j}_S = \bar{Q}_V \mathbf{u} - \frac{k_b T}{Fe} (2t_{(+)} - 1) \nabla \sigma_f.$$

Combining equations 7 and 8, the self-potential field ψ is the solution of the following Poisson equation,

$$\nabla \cdot (\sigma \nabla \psi) = \nabla \cdot \mathbf{j}_S, \tag{13}$$

where the source term (the right-hand side of equation 13) can be directly related to the Darcy velocity field $\mathbf{u}$ and to the gradient of the conductivity of the pore water through equation 12. Both the Darcy velocity and the salinity are obtained by solving equations 1–6 (the so-called primary flow problem) with appropriate boundary conditions.

SANDBOX EXPERIMENT

We performed a sandbox experiment to analyze the self-potential response resulting from the leakage of salty water from a tank into a sandbox. The experimental setup is shown in Figure 1. The sandbox was open at the top and partially filled with a well-sorted silica sand infiltrated with tap water with an electrical resistivity of 650 ohm-m at 20°C. The mean grain radius was 0.35 mm. Prior to introducing the sand into the box, we set up a plastic sheet on the bottom of the sandbox with a network of nonpolarizing electrodes attached to it, covering an area of 12.7 × 7.62 cm (Figure 1a and c). The self-potential signals were monitored with 32 sintered active Ag/AgCl connected to a very sensitive voltmeter initially designed for electroencephalography (Crespy et al., 2008). The electrodes were connected to a precision digital voltmeter having a capacity of as many as 256 sensor-signals digitized with 24-bit resolution. Each channel of the

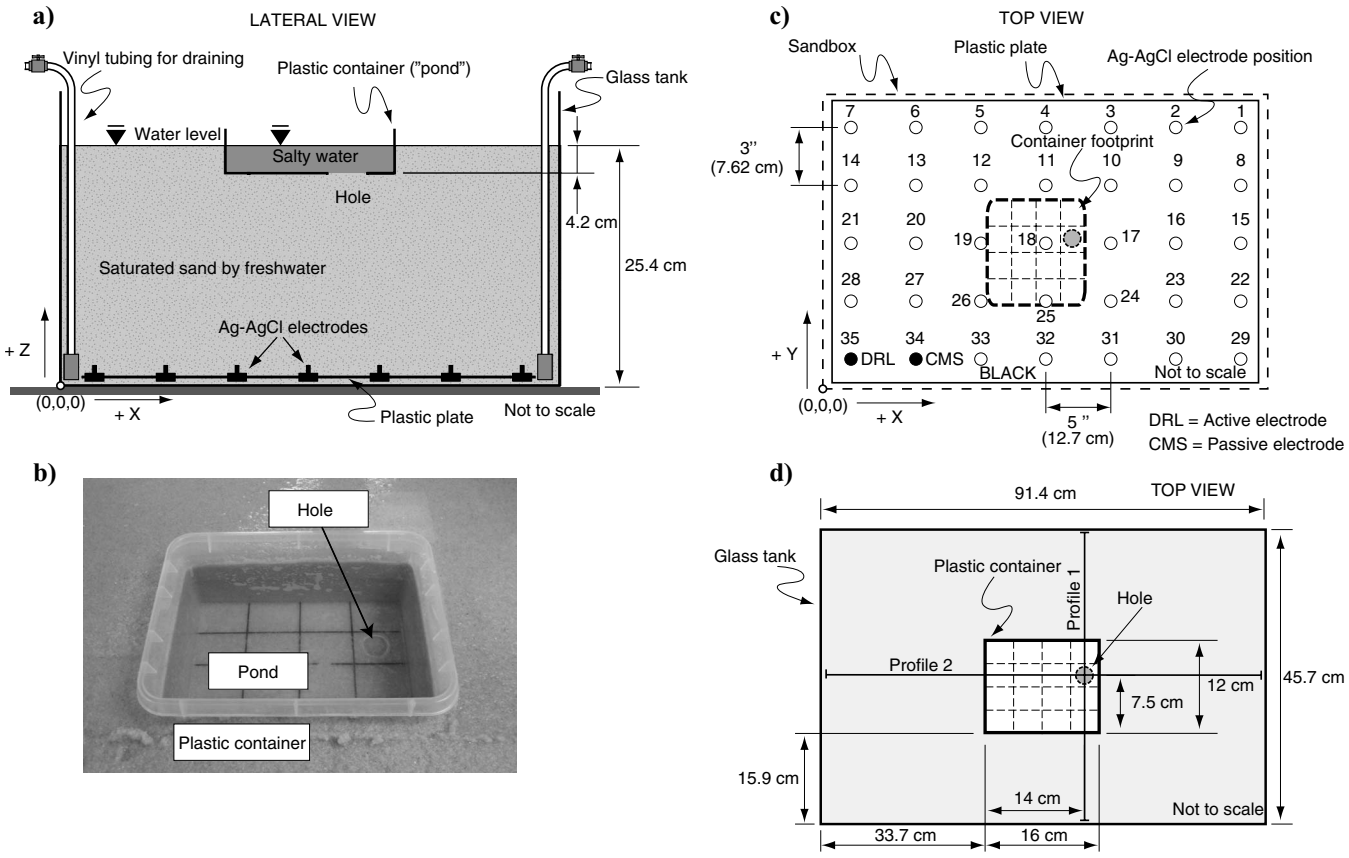

Figure 1. Sketch of the experimental setup. (a) Side view. (b) Picture of the plastic tank. (c, d) Top view with the position of the electrodes. CMS is the reference for the self-potential network of electrodes. Note the position of the two profiles: Profile 1 and Profile 2.

voltmeter consisted of a low-noise DC coupled postamplifier, with a first-order antialiasing filter, followed by a 24-bit Delta-Sigma modulator-based analog-to-digital (AD) converter having an oversampling rate of 64 and a final maximum sampling rate of 2048 Hz, achieved with a postmodulator decimation filter.

The digital output of all the AD converters were digitally multiplexed into a serial data stream and sent to the PC via a single optical fiber through a fiber-to-USB interface without any compression or other form of data reduction. The data were acquired with software that received the serial data, demultiplexed them, and processed them. The software also controlled the voltmeter, displayed the data in real time on a computer screen, and generated BDF formatted data files. Depending on the final data rate selected, decimation might be applied to the received data stream; a fifth-order bidirectional decimation filter might be applied to the data prior to decimation and writing the data out to a file. This voltmeter had a resolution of about 0.1 μV, a maximum frequency of acquisition of 2.048 kHz, and a bandwidth from DC to 400 Hz, with input impedance for the electrodes of 300 Mohm at 50 Hz (see Crespy et al., 2008, and Haas and Revil, 2009, for additional details). For this experiment, a data rate of 128 Hz was chosen, and therefore a postacquisition decimation filter was applied to the data through the data acquisition code. The data were further decimated to a final decimated sample rate of 32 Hz in the data reduction software. This decimation process used the MATLAB internal decimate function using a thirteenth-order Chebyshev type I filter, applied to the data in forward and backward directions to remove phase distortions introduced by the filter.

The sintered electrodes used in the experiment had very low-noise, low-offset voltages, and very stable DC performance. The electrodes had very low output impedance, and therefore all problems with regard to capacitive coupling between the cable and sources of interference were minimized (Crespy et al., 2008). These electrodes also were waterproof and their size was close to 1 mm, so they were treated as point measurements.

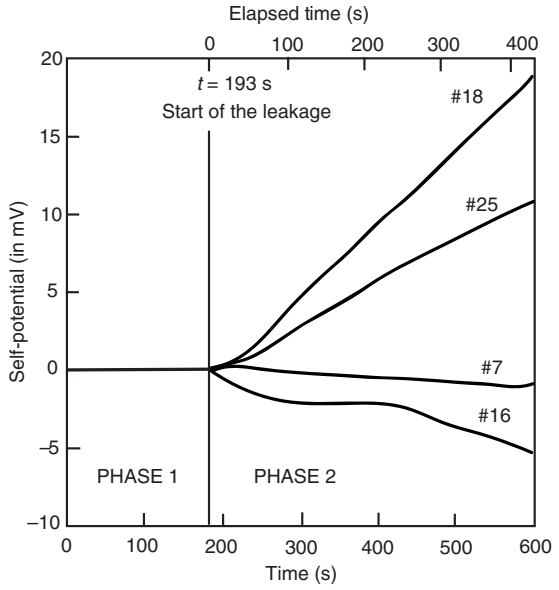

Figure 2. Display of the electrical potentials versus time for some selected electrodes (electrodes 7, 16, 18, and 25; see position Figure 1c) located at the bottom of the sandbox.

Because the data acquisition system was designed to have a large dynamic range, electronic circuits were designed into it to minimize the effects of common-mode signals appearing at the electrode inputs. These circuits use two electrodes, the common-mode sense (CMS) and dynamic reference level (DRL) electrodes. These electrodes are used together in a feedback loop to keep the potential of the sand close to the reference level of the AD converters used in the system. All electrode voltages measured are referenced to the CMS electrode. The DRL electrode is the only driven electrode in the measurement system and provides the signal return path for all of the electrodes with a current limit of 50 μA. These two electrodes form a dynamic reference level circuit that is used in the system to improve common-mode voltage rejection (Figure 1a and c).

On the top of the saturated sand surface, we set up a plastic container, hereafter called the tank. The tank acts as a little pond with an impervious and insulating (plastic) boundary (Figure 1b). This container was placed so that the salty water level inside the tank and the tap water in the sandbox were maintained at the same level (Figure 1b). On the bottom of the tank, a hole was made with a diameter of 1.25 cm (see position in Figure 1). The hole initially was sealed with a sticky tape before starting the measurements. Consequently, the tank did not have any leaks before the start of the measurements.

Prior to removing the tape and starting, the self-potential signals were recorded over 193 s (Figure 2). The signals were stable inside 0.1 mV. In this phase, termed Phase 1, all of the channels had values ranging from -200 μV to $+200$ μV with a constant mean. The second measurement phase (Phase 2 below) started with the opening of the hole (quickly removing the sticky tape covering the hole). This resulted in the formation of a salty plume sinking in the tank. At the start of Phase 2, all the channels showed a significant and progressive change in their self-potential values (Figure 2). The highest changes were recorded approximately below the position of the hole (see Figure 3). Figure 3 shows maps of the self-potential distribution at times 211 s, 303 s, 382 s, and 421 s, respectively (the leakage starts at $t = 193$ s).

SELF-POTENTIAL TOMOGRAPHY

Recently, new self-potential inversion algorithms have emerged using Tikhonov regularization algorithms to reduce the nonuniqueness of the self-potential inverse problem (Linde and Revil, 2007; Minsley et al., 2007a, 2007b; Jardani et al., 2007, 2008; Castermant et al., 2008; Mendonça, 2008; Jardani et al., 2009). We use this type of tomographic algorithm to invert the causative source of the self-potential signals in terms of the source current density. The difference with previous works is that we perform below a time-lapse tomography of the self-potential causative sources to follow the salinity front over time.

We invert the self-potential distribution recorded at the bottom of the sandbox to determine the 3D distribution of the volumetric source current density

$$\mathfrak{I} = \nabla \cdot \mathbf{j}_S, \tag{14}$$

(expressed in A m^{-3}) inside the sandbox. The volumetric source current density distribution corresponds to a vector $\mathbf{m}$ consisting of the model parameters. This implies that at each time step t, we can use as a prior volumetric current density model the model optimized

at time $(t-1)$. Consequently, the cost function to minimize at time t is given by

$$G(t) = (\mathbf{d}(t) - \mathbf{K}\mathbf{m}(t))^{T}\mathbf{W_d}(\mathbf{d}(t) - \mathbf{K}\mathbf{m}(t)) + \lambda(\mathbf{m}(t) - \mathbf{m}(t-1))^{T}\mathbf{W_m}(\mathbf{m}(t) - \mathbf{m}(t-1)), \quad (15)$$

where $\mathbf{K}$ is the kernel of the Poisson operator (see Jardani et al., 2008, for a detailed description of its computation and how to incorporate resistivity information if available);

$$\mathbf{W_d} = \mathrm{diag}\{1/\varepsilon_1, \ldots, 1/\varepsilon_N\} \quad (16)$$

is a square diagonal weighting $N \times N$ matrix (elements along the diagonal of this matrix are the reciprocal of the standard deviation σ_i squared, $\varepsilon_i = \sigma_i^2$); $\mathbf{W}_m$ is the differential Laplacian operator; $\mathbf{m}(t-1)$ represents the vector of the model parameters, that is, the distribution of the volumetric source current density, inverted at time $(t-1)$.

The bulk conductivity is required to compute the correct Poisson kernel for each time-lapse inversion (Jardani et al., 2008). Indeed, the kernel of the Poisson operator in equation 13 is dependent on the bulk conductivity distribution, which must change dramatically with time in the plume area because of the change in the salinity. Errors in the bulk conductivity distribution will lead to errors in source current inversion. However, in the present case we do not know the distribution of the resistivity in the tank. Therefore, to stay conservative we used the resistivity as equal to the background resistivity.

There are two ways to solve this problem. One would be to use a stochastic approach instead of the approach considered here; with such an approach we could simulate the change in the distribution of the resistivity from the change in the distribution of the salinity. The second approach would be to perform a joint inversion of time-lapse electrical resistivity and self-potential data together in the way done by Linde et al. (2006) for georadar and resistivity. However, this would work only for a relatively slow salt-migration process. By this we mean that the characteristic time scale of the salt-migration process needs to be much longer than the time needed to take a resistivity tomography snapshot. For this experiment, the salt migration process is relatively fast compared to the time required to measure the resistivity, and therefore this method is not applicable here.

The initial model is inverted for the location of the volumetric source current density distribution using the result from an extension of the dipolar crosscorrelation algorithm proposed by Revil et al. (2001) and Crespy et al. (2008) while accounting for the boundary conditions of the problem (insulating on all external boundaries). We did not use any other constraints or prior knowledge regarding the position of the hole acting as an initial source of current once opened. The algorithm was written as a MATLAB routine. The solution of the previous problem is given by the minimization of the cost function G with respect to the model parameters. This yields

$$\mathbf{m}_t^{*} = [\mathbf{K}^T(\mathbf{W}_d^T\mathbf{W}_d)\mathbf{K} + \lambda(\mathbf{W}_m^T\mathbf{W}_m)]^{-1}(\mathbf{K}^T(\mathbf{W}_d^T\mathbf{W}_d)\phi_d + \lambda(\mathbf{W}_m^T\mathbf{W}_m)\mathbf{m}_{t-1}). \quad (17)$$

The regularization parameter λ is chosen according to the L-curve criterion (Hansen, 1998).

The results of the time-lapse inversion of the self-potential data are displayed in Figures 4 and 5. Figure 4 shows the full result of the inversion, and Figure 5 shows threshold values in the volumetric current density. At each time step, the fit of the self-potential data was characterized by $R^2 > 0.98$. Figure 5 shows the results of the 3D inversion on two planes that are normal to each other and passing through the position of the hole (see profiles 1 and 2 in Figure 1d). The result of the inversion shows, at each time step, two poles in the volumetric current density. One pole is negative, with values typically between -4 and -7 mA m^{-3}. The contribution of this pole is located along the bottom surface of the tank, and its position agrees

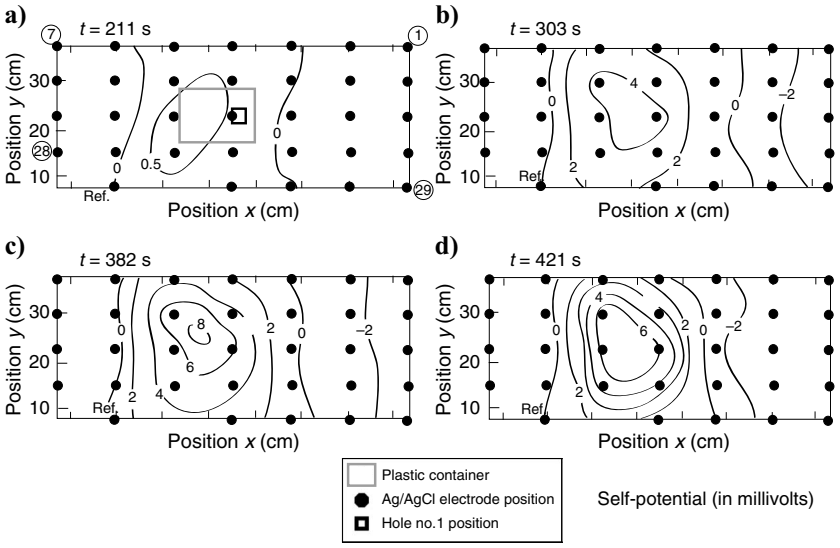

Figure 3. Self-potential maps at the bottom of the tank versus time at four different times following the start of the leak at $t = 193$ s (Phase 2). The distribution before $t = 193$ s is zero everywhere with an uncertainty of 0.2 mV. The abbreviation "Ref" indicates the position of the reference electrode (0 mV). These data show that the saline plume has a positive self-potential signature at the bottom of the tank with a magnitude growing over time.

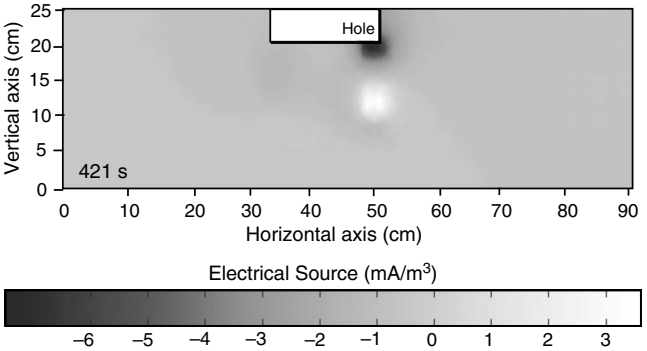

Figure 4. Full result of the inversion showing the distribution of the volumetric source current density at $t = 421$ s after the beginning of the experiment. The leak starts at $t = 193$ s.

with the position of the hole in the tank. The second pole is positive. It has a magnitude that is smaller than the negative pole (typically 0.5 to 3 mA m^{-3}), but its spatial extension is more important. This positive pole is moving downward with time, as shown by Figure 6. The mean velocity is typically 2.5×10^{-4} m s^{-1}. It is tempting to believe that this positive pole is associated with the front of the saline plume and the negative pole with the leak from the tank. This will be discussed in the following section.

DISCUSSION

In this section, we want to determine why the inversion algorithm can retrieve the position of the saline front. Therefore, we performed a 2D numerical model of the self-potential response associated with the transport of a salt plume. We solved equations 1–6 with no source term in equations 2 and 3 ($Q_S = 0$) and using the finite-element method. The initial concentration at the top surface of the system is

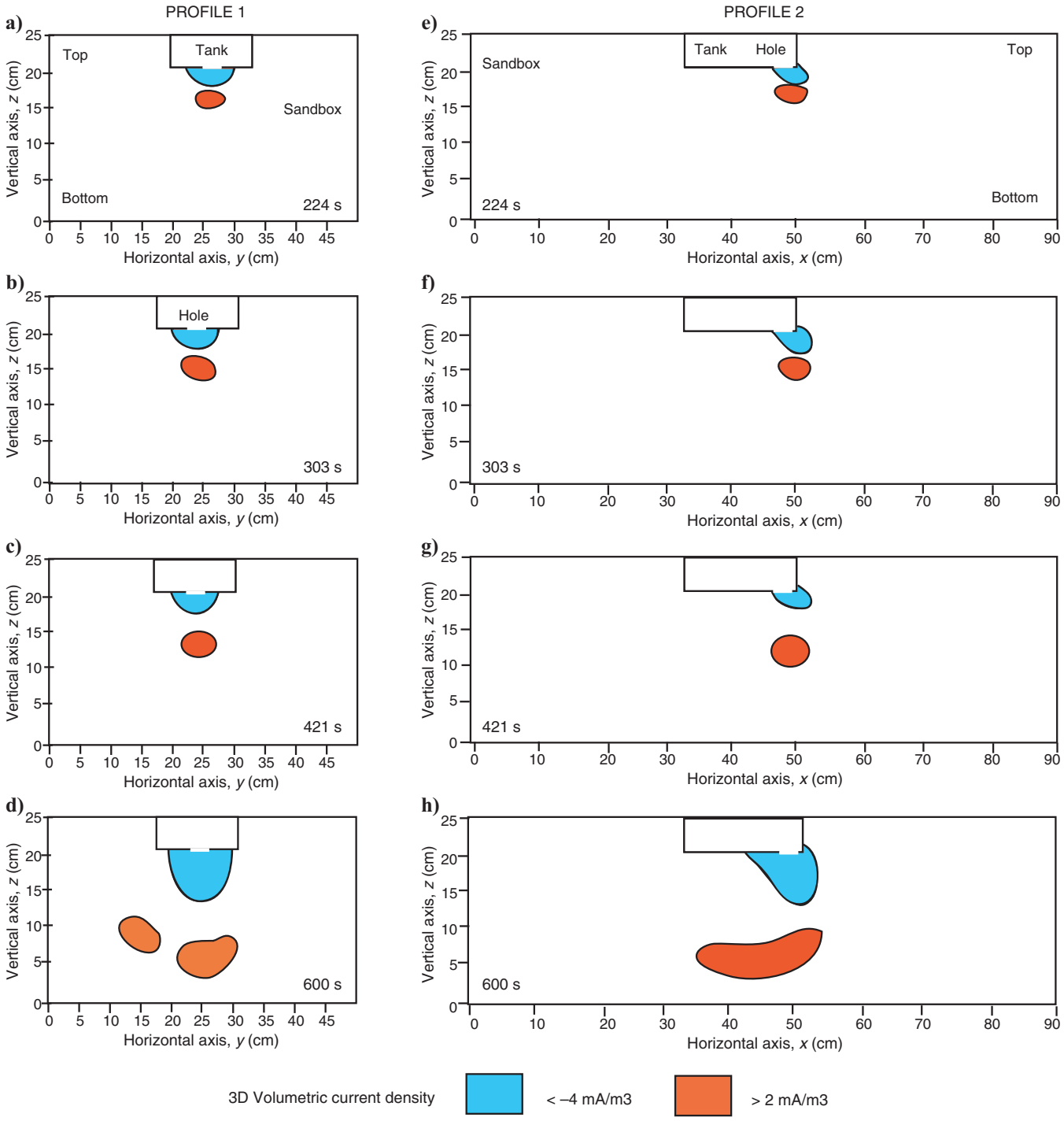

Figure 5. Three-dimensional time-lapse tomography of the source current density resulting from the inversion of the self-potential signals recorded at the bottom of the sandbox. The contour lines correspond to -4 mA/m^3 and 2 mA/m^3 levels in the volumetric current density $\mathfrak{I} = \nabla \cdot \mathbf{j}_S$. Figure 1d shows the positions of profiles 1 and 2.

285.7 kg m^{-3} in the area of leakage. The initial concentration of the salt in the sandbox outside the leaking area is 10 kg m^{-3}. The porosity of the sand in the sandbox is 0.40. The permeability tensor is $\mathbf{k} = k\mathbf{I}$ with $k = 5 \times 10^{-13}$ m^2. The dispersivity is 3.56×10^{-6} m^2 s^{-1}.

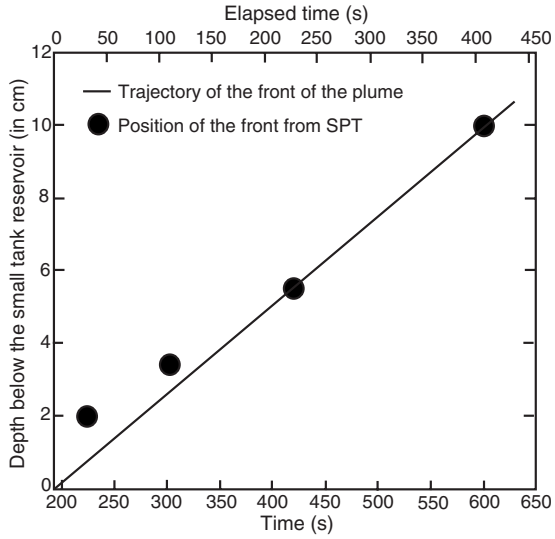

Figure 6. Evolution of the depth of the positive volumetric current density versus elapsed time since the beginning of the leakage. The positive pole of the volumetric source current density is determined from the self-potential tomograms (see Figure 4), and the straight line is determined from the three first tomograms of Figure 4. The depth is considered below the plastic tank containing the saline water. We observe that the positive pole of the volumetric source current density sinks nearly linearly with time. The abbreviation SPT stands for self-potential tomography.

The initial hydrostatic pore pressure is $p = 1010 \times 9.81 \times (0.8 - z)$ (reference pressure), and the side boundaries are considered to be impervious to the flow of the pore water and to the solute.

For the electrical modeling, we used insulating boundary conditions on all boundaries in agreement with the sandbox experiment described in the "Sandbox Experiment" section above. The conductivity of the sand σ was computed from the salinity according to equation 11, where σ_f, the conductivity of the pore water, is known to be directly proportional to the salinity (see, for instance, Revil, 1999). We used a porosity $\phi = 0.38$ (random packing of spherical grains), and $m = 1.3$ (cementation exponent for a sand). The computations were performed with the finite-element code COMSOL Multiphysics 3.5.

Figure 7 shows a plot of the self-potential distribution associated with the plume sinking inside the modeled porous sandbox. The self-potential anomaly is positive in agreement with our experimental result and of the same magnitude. Another result of the numerical modeling consistent with our observations is that the self-potential signals decrease very quickly outside the position of the boundary of the plume. This is consistent with the steady increase of the self-potential response over time observed after the opening of the hole (Figure 2). The numerical simulation was used to compute the volumetric source current density in the sandbox.

The distribution of the source current density is shown in Figure 8. We found that the area of leakage (the source of the salty water plume) is marked by a strong, well-localized, negative pole in the volumetric source current density. The front of the saline plume is characterized by a weak, diffuse, positive pole in the volumetric source current density. This is consistent with the experimental data reported above and analyzed with the time-lapse self-potential tomographic algorithm described above (Figure 5). The slight differ-

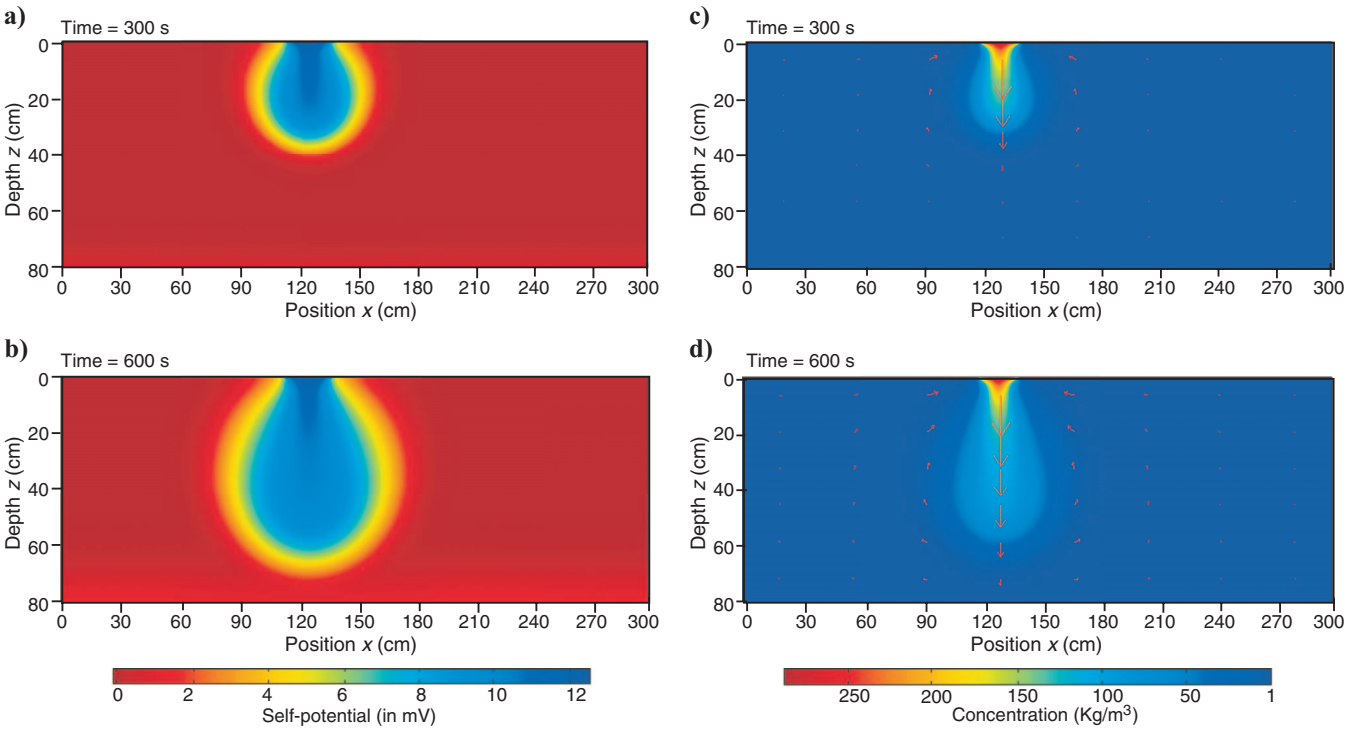

Figure 7. Finite-element simulation of the self-potential signals associated with a sinking salt plume. The self-potential distribution results from both the Darcy's velocity distribution and the diffusion current density associated with the gradient in the electrical conductivity of the pore water. The arrows on the right-hand-side plots represent the Darcy velocity.

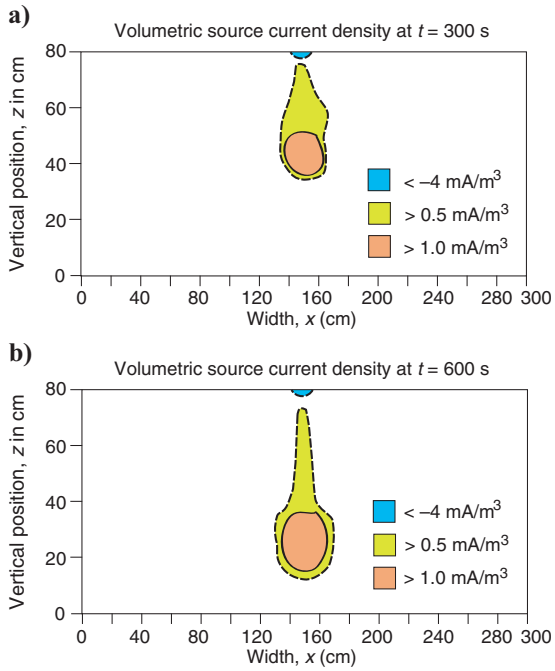

Figure 8. Threshold of the volumetric current density $\Im = \nabla \cdot \mathbf{j}_S$ determined from the 2D forward numerical modeling of a sinking plume of saline water. The sandbox is filled with a sand characterized by isotropic permeability and dispersion tensors and constant porosity.

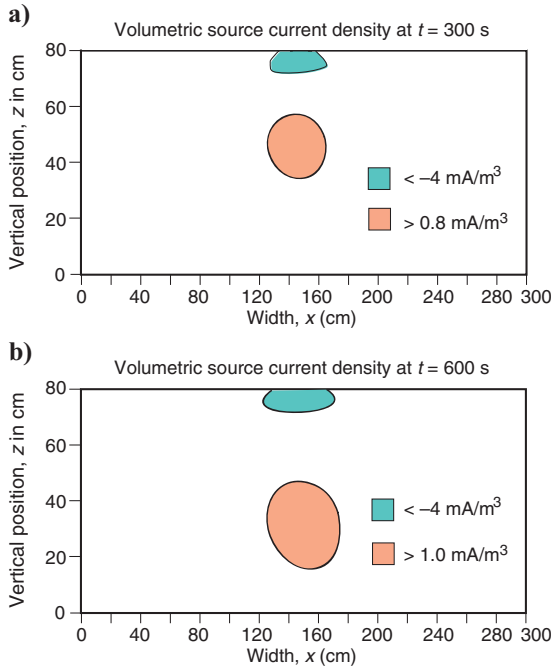

Figure 9. Result of the inversion of the synthetic data. The figure shows the positive and negative thresholds in the value of the volumetric source current density $\Im = \nabla \cdot \mathbf{j}_S$ inverted using the electrical potential information at the bottom of the tank and the time-lapse algorithm described in the main text in the "Self-Potential Tomography" section.

ence in the shape of the volumetric current density might be due to two possibilities: (1) the anisotropy of the permeability and dispersion tensors of the sand in the sandbox, and (2) the fact that we used a constant resistivity for the inversion of the self-potential data.

Figure 9 shows the result of the inversion of the self-potential data computed at the bottom of the sandbox for the synthetic case discussed above. Only threshold values in the volumetric current source density are shown. We took a constant resistivity model for the inversion so that the inverted volumetric source current density ignores the true resistivity distribution of the model. Comparing Figure 8 and Figure 9, we can say that our algorithm works very well in retrieving the position of the leak and the position of the front of the plume. The reason is that the drop in the resistivity distribution is colocated with the position of the boundary of the plume where the current is generated. Thus the true resistivity distribution, in this case, is not of prime importance to locate correctly the source of the self-potential signals.

CONCLUSIONS

A leakage experiment resulting in the formation of a salty water plume was monitored using the self-potential method. From this experiment, the following conclusions have been reached:

1) Clear self-potential signals were measured and shown to result from the plume sinking in the sandbox over time. The amplitude of these anomalies amounted to a few millivolts at the start of the leakage to a few tens of millivolts after a few minutes. Two mechanisms for the generation of these anomalies are the combined streaming potential and the diffusion potential related to the flow of the pore water, and the gradient in the chemical potential of ionic species, respectively.
2) A self-potential tomography algorithm was developed based on Tikhonov regularization and applied to the time-lapse self-potential data to localize the source of current density in the tank.
3) We found that this inversion algorithm produces two types of detections. One is consistent with the position of the leak, and the second can be used to determine the position of the front of the saline plume over time. This result is confirmed by the forward modeling of the whole problem using a finite-element code that simulates the hydrodynamic dispersion of the salt driven by the buoyancy force with the resulting volumetric source current density.

The next step will be to use a more sophisticated stochastic algorithm to invert the transport properties of the porous material using, for instance, a Markov chain Monte-Carlo algorithm. Because resistivity and self-potential data are complementary methods, we expect that the joint time-lapse inversion of self-potential and resistivity data could improve our ability to monitor contaminant plumes in the ground and to predict their future evolutions. In addition, the equations developed in the present paper could be used in a reverse mode to use electro-osmosis for remediation purposes.

ACKNOWLEDGMENTS

We thank Terry Young for his support at the Colorado School of Mines. P. Martínez-Pagán thanks Consejeria de Educacion de la Region de Murcia for funding during his stay at the Colorado School of Mines. This research was supported by the Office of Science (BER), U. S. Department of Energy, Grant No. DE-FG02-08ER646559

"Advanced self-potential tomography." We thank the associate editor Evert Slob, Milenko Burazer, and two anonymous referees for their very useful comments.

REFERENCES

Arora, T., N. Linde, A. Revil, and J. Castermant, 2007, Non-intrusive characterization of the redox potential of landfill leachate plumes from self-potential data: Journal of Contaminant Hydrology, **92**, 274–292.

Aubert, A., and Q. Y. Atangana, 1996, Self-potential method in hydrogeological exploration of volcanic areas: Ground Water, **34**, 1010–1016.

Binley, A., and W. Daily, 2003, The performance of electrical methods for assessing the integrity of geomembrane liners in landfill caps and waste storage ponds: Journal of Environmental and Engineering Geophysics, **8**, 227–237.

Binley, A., W. Daily, and A. Ramirez, 1997, Detecting leaks from environmental barriers using electrical current imaging: Journal of Environmental and Engineering Geophysics, **2**, 11–19.

Birch, F. S., 1993, Testing Fournier's method for finding water table from self-potential: Ground Water, **31**, 50–56.

Bolève, A., A. Crespy, A. Revil, F. Janod, and J. L. Mattiuzzo, 2007, Streaming potentials of granular media: Influence of the Dukhin and Reynolds numbers: Journal of Geophysical Research, **112**, B08204, doi: 10.1029/2006JB004673.

Buselli, G., and K. Lu, 2001, Groundwater contamination monitoring with multichannel electrical and electromagnetic methods: Journal of Applied Geophysics, **48**, 11–23.

Castermant, J., C. A. Mendonça, A. Revil, F. Trolard, G. Bourrié, and N. Linde, 2008, Redox potential distribution inferred from self-potential measurements associated with the corrosion of a burden metallic body: Geophysical Prospecting, **56**, 269–282, doi: 10.1111/j.1365-2478.2007.00675.x.

Crespy, A., A. Bolève, and A. Revil, 2007, Influence of the Dukhin and Reynolds numbers on the apparent zeta potential of granular porous media: Journal of Colloid and Interface Science, **305**, 188–194.

Crespy, A., A. Revil, N. Linde, S. Byrdina, A. Jardani, A. Bolève, and P. Henry, 2008, Detection and localization of hydromechanical disturbances in a sandbox using the self-potential method: Journal of Geophysical Research, **113**, B01205, doi: 10.1029/2007JB005042.

Daily, W., A. Ramirez, and A. Binley, 2004, Remote monitoring of leaks in storage tanks using electrical resistance tomography: Application at the Hanford site: Journal of Environmental and Engineering Geophysics, **9**, 11–24.

Darilek, G., and D. Laine, 2007, Experience with GCLs used as a conductive layer in geomembrane leak-location surveys: Geosynthetics, **25**, 30–35, accessed 28 June 2010, http://geosyntheticsmagazine.com/repository/2/2675/0607gs_digitaledition.pdf.

Fournier, C., 1989, Spontaneous potentials and resistivity surveys applied to hydrogeology in a volcanic area: Case history of the Chaîne des Puys (Puy-de-Dôme, France): Geophysical Prospecting, **37**, 647–668.

Fox, R. W., 1830, On the electro-magnetic properties of metalliferous veins in the mines of Cornwall: Philosophical Transaction of the Royal Society, **120**, 399–414.

Frangos, W., 1997, Electrical detection of leaks in lined waste disposal ponds: Geophysics, **62**, 1737–1744.

Haas, A., and A. Revil, 2009, Electrical burst signature of pore-scale displacements: Water Resources Research, **45**, W10202, doi: 10.1029/2009WR008160.

Hämmann, M., H. R. Maurer, A. G. Green, and H. Horstmeyer, 1997, Self-potential image reconstruction: Capabilities and limitations: Journal of Environmental and Engineering Geophysics, **2**, 21–35.

Hansen, P. C., 1998, Rank-deficient and discrete ill-posed problems: Numerical aspects of linear inversion: Society for Industrial and Applied Mathematics.

Jardani, A., A. Revil, W. Barrash, A. Crespy, E. Rizzo, S. Straface, M. Cardiff, B. Malama, C. Miller, and T. Johnson, 2009, Reconstruction of the water table from self-potential data: A Bayesian approach: Ground Water, **47**, 213–227.

Jardani, A., A. Revil, A. Bolève, and J. P. Dupont, 2008, Three-dimensional inversion of self-potential data used to constrain the pattern of groundwater flow in geothermal fields: Journal of Geophysical Research, **113**, B09204, doi: 10.1029/2007JB005302.

Jardani, A., A. Revil, A. Bolève, J. P. Dupont, W. Barrash, and B. Malama, 2007, Tomography of groundwater flow from self-potential (SP) data: Geophysical Research Letters, **34**, L24403, doi: 10.1029/2007GL031907.

Linde, N., A. Binley, A. Tryggvason, L. B. Pedersen, and A. Revil, 2006, Improved hydrogeophysical characterization using joint inversion of cross-hole electrical resistance and ground-penetrating radar traveltime data: Water Resources Research, **42**, W12404, doi: 10.1029/2006WR005131.

Linde, N., and A. Revil, 2007, Inverting self-potential data for redox potentials of contaminant plumes: Geophysical Research Letters, **34**, L14302, doi: 10.1029/2007GL030084.

Maineult, A., Y. Bernabé, and P. Ackerer, 2004, Electrical response of flow, diffusion, and advection in a laboratory sand box: Vadose Zone Journal, **3**, 1180–1192.

———, 2005, Detection of advected concentration and pH fronts from self-potential measurements: Journal of Geophysical Research, **110**, B11205, doi: 10.1029/2005JB003824.

———, 2006, Detection of advected, reacting redox fronts from self-potential measurements: Journal of Contaminant Hydrology, **86**, 32–52.

Malama, B., K. L. Kuhlman, and A. Revil, 2009a, Theory of transient streaming potentials associated with axial-symmetric flow in unconfined aquifers: Geophysical Journal International, **179**, 990–1003, doi: 10.1111/j.1365-246X.2009.04336.x.

Malama, B., A. Revil, and K. L. Kulhman, 2009b, A semi-analytical solution for transient streaming potentials associated with confined aquifer pumping tests: Geophysical Journal International, **176**, 1007–1016, doi: 10.1111/j.1365-246X.2008.04014.x.

Mendonça, C. A., 2008, Forward and inverse self-potential modeling in mineral exploration: Geophysics, **73**, no. 1, F33–F43.

Minsley, B. J., J. Sogade, and F. D. Morgan, 2007a, Three-dimensional self-potential inversion for subsurface DNAPL contaminant detection at the Savannah River site, South Carolina: Water Resources Research, **43**, W04429, doi: 10.1029/2005WR003996.

———, 2007b, Three-dimensional source inversion of self-potential data: Journal of Geophysical Research, **112**, B02202, doi: 10.1029/2006JB004262.

Naudet, V., A. Revil, J.-Y. Bottero, and P. Bégassat, 2003, Relationship between self-potential (SP) signals and redox conditions in contaminated groundwater: Geophysical Research Letters, **30**(21), 2091, doi: 10.1029/2003GL018096.

Naudet, V., A. Revil, E. Rizzo, J.-Y. Bottero, and P. Bégassat, 2004, Groundwater redox conditions and conductivity in a contaminant plume from geoelectrical investigations: Hydrology and Earth System Sciences, **8**, 8–22.

Oltean, C., and M. A. Buès, 2002, Infiltration of salt solute in homogeneous and saturated porous media — An analytical solution evaluated by numerical simulations: Transport in Porous Media, **48**, 61–78.

Parra, J. O., 1988, Electrical response of a leak in a geomembrane liner: Geophysics, **53**, 1445–1452.

Parra, J. O., and T. E. Owen, 1988, Model studies of electrical leak detection surveys in geomembrane-lined impoundments: Geophysics, **53**, 1453–1458.

Perry, J. W., C. E. Corry, and T. Madden, 1996, Monitoring leakage from underground storage tanks using spontaneous polarization (SP) method: 66th Annual International Meeting, SEG, Expanded Abstracts, 932–935.

Revil, A., 1999, Ionic diffusivity, electrical conductivity, membrane and thermoelectric potentials in colloids and granular porous media: A unified model: Journal of Colloid and Interface Science, **212**, 503–522.

Revil, A., M. Darot, and P. A. Pezard, 1996, Influence of the electrical diffuse layer and microgeometry on the effective ionic diffusion coefficient in porous media: Geophysical Research Letters, **23**, 1989–1992.

Revil, A., L. Ehouarne, and E. Thyreault, 2001, Tomography of self-potential anomalies of electrochemical nature: Geophysical Research Letters, **28**, 4363–4366.

Revil, A., and P. Leroy, 2001, Hydroelectric coupling in a clayey material: Geophysical Research Letters, **28**, 1643–1646.

———, 2004, Constitutive equations for ionic transport in porous shales: Journal of Geophysical Research, **109**, B03208, doi: 10.1029/2003JB002755.

Revil, A., P. Leroy, and K. Titov, 2005, Characterization of transport properties of argillaceous sediments: Application to the Callovo-Oxfordian Argillite: Journal of Geophysical Research, **110**, B06202, doi: 10.1029/2004JB003442.

Revil, A., and N. Linde, 2006, Chemico-electromechanical coupling in microporous media: Journal of Colloid and Interface Science, **302**, 682–694.

Revil, A., F. Trolard, G. Bourrié, J. Castermant, A. Jardani, and C. A. Mendonça, 2009, Ionic contribution to the self-potential signals associated with a redox front: Journal of Contaminant Hydrology, **109**, 27–39.

Sill, W. R., 1983, Self-potential modeling from primary flows: Geophysics, **48**, 76–86.

Suski, B., E. Rizzo, and A. Revil, 2004, A sandbox experiment of self-potential signals associated with a pumping test: Vadose Zone Journal, **3**, 1193–1199.

Weigel, M., 1989, Self-potential surveys on waste dumps: Theory and practice, *in* G.-P. Merkler, H. Militzer, H. Hötzl, H. Armbruster, and J. Brauns, eds., Detection of subsurface flow phenomena: Lecture Notes in Earth Science, **27**, 109–120, doi: 10.1007/BFb0011626.